

Valley modulation and topological phase transition in staggered kagome ferromagnets

Yuheng Xing(邢玉恒), Wenjuan Qiu(邱文娟), Xinxing Wu(吴新星), and Yue Tan(谭悦)
Citation: Chin. Phys. B, 2024, 33 (**12**): 127503. DOI: 10.1088/1674-1056/ad7af7
Journal homepage: http://cpb.iphy.ac.cn; http://iopscience.iop.org/cpb

What follows is a list of articles you may be interested in

Dzyaloshinskii-Moriya interaction and field-free sub-10 nm topological magnetism in Fe/bismuth oxychalcogenides heterostructures

Yaoyuan Wang(王垚元), Long You(游龙), Kai Chang(常凯), and Hongxin Yang(杨洪新)
Chin. Phys. B, 2024, 33 (**9**): 097508. DOI: 10.1088/1674-1056/ad6a0e

Interacting topological magnons in a checkerboard ferromagnet

Heng Zhu(朱恒), Hongchao Shi(施洪潮), Zhengguo Tang(唐政国), and Bing Tang(唐炳)
Chin. Phys. B, 2024, 33 (**3**): 037503. DOI: 10.1088/1674-1056/ad01a2

Oscillation of Dzyaloshinskii-Moriya interaction driven by weak electric fields

Runze Chen(陈润泽), Anni Cao(曹安妮), Xinran Wang(王馨苒), Yang Liu(柳洋), Hongxin Yang(杨洪新), and Weisheng Zhao(赵巍胜)
Chin. Phys. B, 2024, 33 (**2**): 027501. DOI: 10.1088/1674-1056/ad0f85

Influence of Dzyaloshinskii-Moriya interaction on the magnetic vortex reversal in an off-centered nanocontact geometry

Hua-Nan Li(李化南), Tong-Xin Xue(薛彤鑫), Lei Chen(陈磊), Ying-Rui Sui(隋瑛瑞), and Mao-Bin Wei(魏茂彬)†
Chin. Phys. B, 2022, 31 (**9**): 097501. DOI: 10.1088/1674-1056/ac4cbd

Synchronization of nanowire-based spin Hall nano-oscillators

Biao Jiang(姜彪), Wen-Jun Zhang(张文君), Mehran Khan Alam, Shu-Yun Yu(于淑云), Guang-Bing Han(韩广兵), Guo-Lei Liu(刘国磊), Shi-Shen Yan(颜世申), and Shi-Shou Kang(康仕寿)
Chin. Phys. B, 2022, 31 (**7**): 077503. DOI: 10.1088/1674-1056/ac560a

---

Valley modulation and topological phase transition in staggered kagome ferromagnets

Yuheng Xing(邢玉恒), Wenjuan Qiu(邱文娟), Xinxing Wu(吴新星)[†], and Yue Tan(谭悦)[‡]

Department of Physics, School of Mathematics and Physics, Yancheng Institute of Technology, Yancheng 224051, *China*

(Received 17 June 2024; revised manuscript received 31 August 2024; accepted manuscript online 14 September 2024)

Owing to their charge-free property, magnons are highly promising for achieving dissipationless transport without Joule heating, and are thus potentially applicable to energy-efficient devices. Here, we investigate valley magnons and associated valley modulations in a kagome ferromagnetic lattice with staggered exchange interaction and Dzyaloshinskii–Moriya interaction. The staggered exchange interaction breaks the spatial inversion symmetry, leading to a valley magnon Hall effect. With nonzero Dzyaloshinskii–Moriya interaction in a staggered kagome lattice, the magnon Hall effect can be observed from only one valley. Moreover, reversing the Dzyaloshinskii–Moriya interaction ($D \to -D$) and exchanging J_1 and J_2 ($J_1 \leftrightarrow J_2$) can also regulate the position of the unequal valleys. With increasing Dzyaloshinskii–Moriya interaction, a series of topological phase transitions appear when two bands come to touch and split at the valleys. The valley Hall effect and topological phase transitions observed in kagome magnon lattices can be realized in thin films of insulating ferromagnets such as $Lu_2V_2O_7$, and will extend the basis for magnonics applications in the future.

Keywords: valley modulation, Dzyaloshinskii–Moriya interaction, staggered kagome ferromagnets, topological phase transitions, magnon Hall effect

PACS: 75.30.Ds, 75.47.–m, 75.70.Ak, 85.75.–d **DOI:** 10.1088/1674-1056/ad7af7

1. Introduction

The magnon Hall effect, due to the Dzyaloshinskii–Moriya interaction (DMI) that plays the role of a vector potential similar to the Lorentz force,[1,2] has been theoretically predicted and experimentally observed in magnetic insulators.[3,4] For the magnon Hall effect in two-dimensional (2D) ferromagnets, the magnon bands can indeed be topologically nontrivial with nonzero Chern numbers.[3,5] However, it can also occur in collinear antiferromagnets where the DMI does not affect the band topology.[6,7] In addition, various topologically nontrivial properties have been explored in kagome lattice systems, such as topological magnon insulators,[8] which exhibit many analogous features to electronic topological insulators.[9,10] Due to the potential to achieve dissipationless transport, the topological behavior of magnons has attracted many investigations in insulating magnets.[11–15] Since magnons can transfer and process information without dissipative ohmic loss,[16] previous works have proposed using magnetic excitations as a platform for realizing analogs of other topological systems, such as Dirac semimetals[17,18] and Weyl semimetals.[19,20] Besides, for ferromagnetically ordered systems, topological magnons have been theoretically proposed in honeycomb lattices,[21,22] kagome lattices,[3,12,15,23,24] pyrochlore lattices[8] and skyrmion lattices.[25] For antiferromagnets, topological magnons also appear in pyrochlore lattices,[20] square lattices[26] and cubic lattices.[13]

In electronics, the finding of contrasting electronic physics in valleys of honeycomb lattices opens a new field of valleytronics in condensed matter physics;[27] the valley degrees of freedom also have enormous potential in valley-dependent photo-electrons and coupled spin valley physics apart from charge and spin.[28–30] Using valley degree of freedom as an information carrier is a rising field in condensed matter physics. The theoretically proposed valley Hall effect has been demonstrated in monolayer MoS_2 transistors,[31,32] graphene superlattices,[33] honeycomb lattices and Lieb lattices.[34–36] It was experimentally observed in pyrochlore structure materials with kagome layers, such as $In_2Mn_2O_7$, $Ho_2V_2O_7$ and $Lu_2V_2O_7$. [37,38] Furthermore, in CrI_3-based van der Waals heterostructures, magnons exhibit a nontrivial topological band structure without DMI, leading to a topological magnon valley current.[39,40] The exploration of valleytronics and topological magnons not only holds conceptual importance in fundamental quantum physics but also has potential applications in advanced information technology.

In this paper, we investigate valley magnons and their topological properties with staggered exchange interaction (SEI) and DMI. Similar to DMI, SEI in neighboring triangles of a kagome lattice (as shown in Fig. 1) creates gaps at $\boldsymbol{K}$ and $\boldsymbol{K}'$ valleys and retains valley degeneracy. Due to the stacking structure of a pyrochlore lattice of an insulating ferromagnet, we can introduce a kagome AB lattice with broken inversion symmetry. In a kagome AB lattice, when the DMI is nonzero the energy gap at one valley will shrink while the gap around the other valley will expand; thus a valley Hall effect appears. Moreover, when exchanging the two nearest-neighbor couplings of J_1 and J_2, the position of non-equivalent

[†]Corresponding author. E-mail: wuxinxing@ycit.edu.cn
[‡]Corresponding author. E-mail: tanyue@ycit.edu.cn

© 2024 Chinese Physical Society and IOP Publishing Ltd

energy valleys in the Brillouin zone will change too. Through a magnon waveguide one can observe a specific valley Hall effect around the shrinking gap. The shrinking gap tends to close and open again with increasing DMI, when a topological phase transition appears. In addition, a series of topological phase transitions can be observed in the large range of the DMI.

2. Spin-wave Hamiltonian

The magnon Hall effect was observed in the insulating ferromagnet $Lu_2V_2O_7$ with a pyrochlore lattice,[38] in which the magnetic atom vanadium has stacking of alternating kagome and triangular lattices along the [111] direction, as shown in Fig. 1(a). To study magnon transport in a ferromagnetic insulator, the effective Hamiltonian can be written as[1,2,5,8,15,38–48]

$$H = \sum_{\langle mn\rangle}[-J_{mn}\boldsymbol{S}_m\cdot\boldsymbol{S}_n+\boldsymbol{D}_{mn}\cdot(\boldsymbol{S}_m\times\boldsymbol{S}_n)] - g\mu_{\mathrm{B}}\boldsymbol{H}_0\cdot\sum_n\boldsymbol{S}_n, \tag{1}$$

where $\boldsymbol{S}_n$ is the spin angular momentum at site n, $-J_{mn}$ denotes the nearest-neighbor coupling, $\boldsymbol{D}_{mn}$ denotes the DM vector between sites m and n and the last term comes from the Zeeman effect in the presence of an external magnetic field $\boldsymbol{H}_0$. g and μ_{B} denote the g factor of electrons and the Bohr magneton, respectively. With the magnetic field along the [111] direction, the magnon Hall effect only comes from the non-cancellation of different types of loops of DMI in the unit cell of the kagome lattice,[38,49–51] as shown in Fig. 1(b). Thus, the kagome sublattice structure plays a key role in the presence of the magnon Hall effect in $Lu_2V_2O_7$. Then, using the Holstein–Primakoff transformation,[52,53] we can obtain the quadratic spin wave Hamiltonian

$$H = -\sum_{\langle mn\rangle}(b_m^{\dagger}H_{mn}b_n+E_0). \tag{2}$$

Here, $b^{\dagger}$ is the bosonic creation operator corresponding to magnons, $H_{mn}=(J_{mn}\pm\mathrm{i}\boldsymbol{D}_{mn})S$, $H_{nm}=(J_{nm}\mp\mathrm{i}\boldsymbol{D}_{nm})S$ and $H_{mm}=\sum_{m=1}^{M_n}J_{mn}S+hS$ and M_n is the number of nearest neighbors of the site n. The ground-state energy of the system is $E_0=-S^2\sum_{n=1}^{N}\sum_{m=1}^{M_n}J_{mn}-NhS$, N is the total number of sites and $h=g\mu_{\mathrm{B}}H_0$. We set $J_{mn}=J$, $D_{mn}=D$ and the kagome lattice with DMI is shown in Fig. 1(a).

We know that the magnon Hall effect has been experimentally observed in a pyrochlore lattice of $Lu_2V_2O_7$ in which the magnetic atom vanadium has a corner-sharing tetrahedral sublattice, as in Fig. 1(a) which shows three layers with the middle layer being a kagome lattice. The two outermost triangular lattices connect to the sublattices A and B of the kagome lattice (as shown in Fig. 1(b)), respectively. Since all the projections of the DMI between interlayer sites are zero, we can regard the DMI for sublattices A and B as the same; however, the ferromagnetic exchange coupling in sublattices A and B can be different. Generally, we can use the symbols J_1 and J_2 to mark different ferromagnetic exchange couplings in triangles A and B, satisfying $J_1=J_2\cdot\gamma$, where the parameter γ is introduced to describe the anisotropy of the system. If $\gamma=1$, the two nearest-neighbor couplings of J_1 and J_2 are equal, which means that the spatial inversion symmetry of the kagome system is preserved. Otherwise, for $\gamma\neq1$, the spatial inversion symmetry is broken. A special case is a bilayer structure containing one kagome layer and one triangular layer, which exhibits a valley structure in quasiparticle spectra. Without loss of generality, we use dimensionless units and set $S=1/2$, $J=1$ for the model calculation. Since the magnetic field decides the direction of spins at the ground state, and the induced Zeeman effect term shifts the dispersion relation, here we set $H_0=0$[†]. Equation (2) resembles the tight-binding model, and each unit cell has three sites, thus we can do the Fourier transformation as

$$b_{\boldsymbol{R}_l+\boldsymbol{r}_m}=\frac{1}{N_u}\sum_{\boldsymbol{k}}\mathrm{e}^{-\mathrm{i}\boldsymbol{k}(\boldsymbol{R}_l+\boldsymbol{r}_m)}b_m(\boldsymbol{k}). \tag{3}$$

Here, N_u is the number of unit cells and $\boldsymbol{R}_l+\boldsymbol{r}_m$ is the spatial position of the mth site in the nth unit cell. Thus, the spin wave Hamiltonian in momentum space can be rewritten as

$$H_{\mathrm{SW}}(\boldsymbol{k})=\begin{pmatrix}H_0 & H_{12}(\boldsymbol{k}) & H_{13}(\boldsymbol{k})\\ H_{12}^*(\boldsymbol{k}) & H_0 & H_{23}(\boldsymbol{k})\\ H_{13}^*(\boldsymbol{k}) & H_{23}^*(\boldsymbol{k}) & H_0\end{pmatrix} \tag{4}$$

with $H_0=2(1+\gamma)JS$, $H_{12}(\boldsymbol{k})=-K_+\mathrm{e}^{-\mathrm{i}\phi_1}-K'_+\mathrm{e}^{-\mathrm{i}\phi_1}$, $H_{13}(\boldsymbol{k})=-K_-\mathrm{e}^{-\mathrm{i}\phi_2}-K'_-\mathrm{e}^{-\mathrm{i}\phi_2}$, $H_{23}(\boldsymbol{k})=-K_+\mathrm{e}^{-\mathrm{i}\phi_3}-K'_+\mathrm{e}^{-\mathrm{i}\phi_3}$, $K_\pm=J\pm\mathrm{i}D$, $K'_\pm=\gamma J\pm\mathrm{i}D$, $\phi_1=\frac{\sqrt{3}a}{4}k_x-\frac{a}{4}k_y$, $\phi_2=\frac{\sqrt{3}a}{4}k_x+\frac{a}{4}k_y$ and $\phi_3=\frac{a}{2}k_y$. Also, a is equal to twice the site spacing.

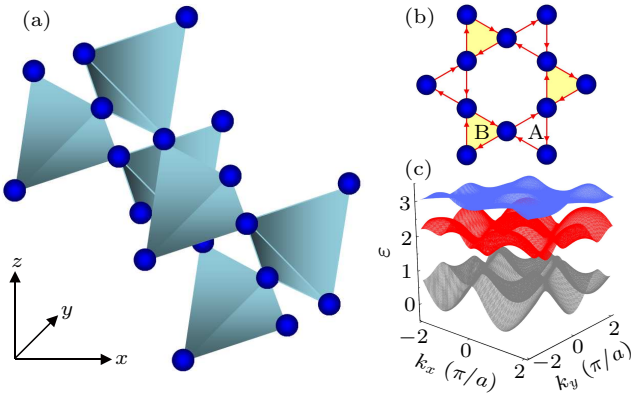


Fig. 1. (a) Schematic diagram of the pyrochlore crystallographic structure–stacking of alternating kagome (the middle layer) and triangular lattices (two outmost layers) along the [111] direction. (b) A kagome AB lattice with DMI; the coupling of two sites along the arrows is $(J_{mn}+\mathrm{i}D)S$, and in the opposite direction corresponds to $(J_{mn}-\mathrm{i}D)S$; triangles A and B have different ferromagnetic exchange couplings of J_1 and J_2, respectively. (c) Magnon dispersion relation of a kagome lattice with $D=0.2J$, $J_1=J_2=1$, $S=1/2$.

According to the standard method for calculating the magnon Berry phase,[5,8] we can obtain the Berry curvature

in the momentum space as

$$\Omega^n_{k_xk_y} = \mathrm{i}\sum_{n'\neq n}\frac{\varphi_n^\dagger\frac{\partial H_{\mathrm{SW}}}{\partial k_x}\varphi_{n'}\varphi_{n'}^\dagger\frac{\partial H_{\mathrm{SW}}}{\partial k_y}\varphi_n - (k_x\leftrightarrow k_y)}{(\varepsilon_n-\varepsilon_n')^2}. \quad (5)$$

To gain a better understanding of the topological phase transitions, we further calculate the Chern numbers of three bands as invariants of topological phase transitions. As a result, the Chern number can be given by the integration of the Berry curvature over the first Brillouin zone as

$$C^n = \frac{1}{2\pi}\iint_{\mathrm{BZ}}\mathrm{d}k_x\mathrm{d}k_y\Omega^n_{k_xk_y}, \quad (6)$$

where ε_n and φ_n are the eigenvalue and eigenvector of the nth band, respectively.

3. Band structure and topological phase transition

Because there are three sites in each kagome unit cell (see Fig. 1(b)), there are three energy bands separated by two energy gaps. In a uniform kagome lattice ($\gamma = 1$) with DMI, the magnon dispersion relation exhibits a threefold rotational symmetry. When the DMI is zero, the top band is flat and there is a degenerate point at the Γ point for the top and middle bands, as shown in Fig. 2(a) (solid lines). The Chern numbers of the three bands are zero, which means that if $D = 0$ all bands including the top flat band are topologically trivial. If DMI is nonzero, a gap between the top and middle bands opens at the Γ point, as shown in Fig. 1(c), and the Chern numbers of the top band and the bottom band jump to 1 and -1, respectively. The top band is not purely flat, and its band width will enlarge with increasing DMI.[46,47] In the weak DMI regime, the band width is not so large that the top band can be regarded as quite flat, which is experimentally observed in a ferromagnetic material Cu(1,3-benzenedicarboxylate).[15]

In the kagome AB lattice ($\gamma \neq 1$) with nonuniform exchange coupling, the degeneracy of the middle and bottom bands at Brillouin zone corners $\boldsymbol{K}$ and $\boldsymbol{K}'$ is removed and a gap is open, as shown in Fig. 2 (inset (a)). With the gap being open, for the bottom and middle bands the valleys $\boldsymbol{K}$ $\left(\frac{4\pi}{3a}\right)$ and $\boldsymbol{K}'$ $\left(-\frac{4\pi}{3a}\right)$ have opposite Berry curvatures. As shown in the contour plot of Berry curvature in wave vector space (Fig. 2, inset (b)), two kinds of valleys $\boldsymbol{K}$ and $\boldsymbol{K}'$ have very contrasting opposite Berry curvatures, which is exactly the same as for the valley Hall effects in electronic and phononic honeycomb lattices.[27,54] The opposite Berry curvatures at $\boldsymbol{K}$ and $\boldsymbol{K}'$ endow the magnons with opposite anomalous velocities, and thus induce Hall effects along different directions. Since the energies of magnons at $\boldsymbol{K}$ and $\boldsymbol{K}'$ in one band are degenerate the Hall currents from the two valleys will cancel each other and the total Hall current will also vanish.

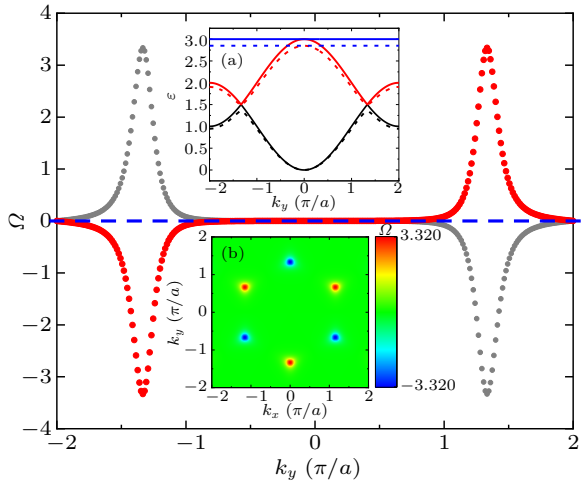


Fig. 2. The Berry curvature of the three magnon bands for a kagome AB lattice with $\gamma = 0.8$ and zero DMI. Inset (a) shows the magnon dispersion relation for a uniform kagome lattice ($\gamma = 1$, solid lines) and a kagome AB lattice ($\gamma = 0.8$, dotted lines) while inset (b) shows a contour plot for Berry curvature of the middle magnon band at $D = 0$ and $\gamma = 1$.

With nonzero DMI in the kagome AB lattice, the degeneracy of valleys $\boldsymbol{K}$ and $\boldsymbol{K}'$ in each band is removed, and thus the gaps between the middle and bottom bands at $\boldsymbol{K}$ and $\boldsymbol{K}'$ are different, as shown in Fig. 3(a). The nonzero DMI makes the middle and top bands topologically nontrivial, while the bottom band is topologically trivial with zero Chern number, as can be seen from Fig. 3(f). As shown in Fig. 3(b), at the $\boldsymbol{K}$ point, the middle and bottom bands have opposite contrasting Berry curvatures. In this system, the direct band gap appears at the wave vector of $\boldsymbol{K}$; thus, by using a magnon waveguide to only allow magnons with energy around the band gap to transmit through the system one can observe nonzero magnon valley Hall current from valley $\boldsymbol{K}$ due to the its contrasting Berry curvature. At valley $\boldsymbol{K}$, the magnons in the bottom and middle bands have Hall currents with opposite directions. If the DMI changes sign one can observe an opposite valley Hall current at $\boldsymbol{K}'$ from the magnons near the band gap.

For a kagome AB lattice with a larger DMI, the gap at $\boldsymbol{K}$ becomes smaller while the gap at $\boldsymbol{K}'$ increases. When the DMI is increased to about $D = 0.175J$ at $\gamma = 0.8$, the gap at $\boldsymbol{K}$ closes and then opens again, as shown Fig. 3(e). The Berry curvature at $\boldsymbol{K}$ reverses when the gap closes and opens again (see Figs. 3(b) and 3(d)); thus, the band topology changes, i.e., the Chern numbers of the middle and bottom bands exchange at DMI around $D = 0.175J$. In other words, a topological phase transition of magnons appears in the kagome AB lattice, as shown in Fig. 3(f). Furthermore, if the sign of DMI reverses, the energy gap between the middle and bottom bands will be close and open around $D = -0.175J$. A topological phase transition appears too and the band Chern numbers are odd functions of the DMI. Thus, we only discuss the positive DMI later.

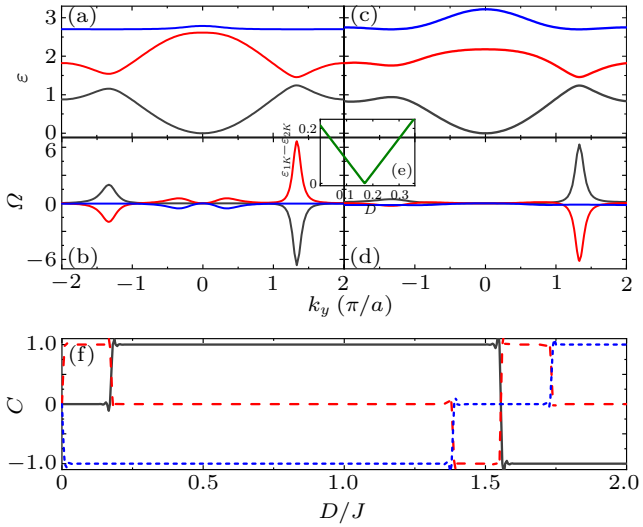


Fig. 3. The dispersion relations ((a) and (c)) and the corresponding Berry curvatures ((b) and (d)) for a kagome AB lattice with different DMIs ($D = 0.05J$ and $D = 0.3J$). (e) The energy gap between the middle band and the lower one at the $\boldsymbol{K}$ point ($k_x = 0$; $k_y = \left(\frac{4\pi}{3a}\right)$). (f) The Chern numbers of the three magnon bands versus the strength of the DMI. Here $\gamma = 0.8$ for in parts (a)–(f).

Unlike the uniform kagome lattice where topological phase transition appears at $D = \sqrt{3}/3J$ in addition to one at $D = 0$, for a kagome AB lattice with $\gamma = 0.8$, in addition to the topological phase transition around $D = 0.175J$ we can also find another three topological phase transitions within the range of $D < 2J$. Each topological phase transition corresponds to two bands touching and splitting with exchange of their Chern numbers, as shown in Fig. 3(f). Except for the topological phase transition around $D = 1.56J$, where the middle and bottom bands touch around the Γ point, all the others correspond to touching and splitting at valleys $\boldsymbol{K}$ and $\boldsymbol{K}'$. For the two bands touching at valleys $\boldsymbol{K}$ and $\boldsymbol{K}'$, their Chern numbers have a difference of 1 (that is, one is 0 another is ± 1), and the integral of Berry curvatures around the valley before touching is ± 0.5, which changes sign after touching and splitting; thus, the Chern numbers have a change of ∓ 1 and the two bands exchange their Chern numbers.

With breakage of the spatial inversion symmetry, $\Omega(k)$ becomes nonvanishing and has opposite extrema with the same magnitude at the $\boldsymbol{K}$ and $\boldsymbol{K}'$ valleys for the middle band. The Chern number, as the integral quantity of $\Omega(k)$, is thus zero, as shown in Fig. 4. Although the magnon band is topologically trivial, opposite $\Omega(k)$ and $\Omega(-k)$ endow valley magnons with opposite anomalous velocities, and consequently induce transverse Hall heat currents along opposite directions (this is a magnon version of the valley Hall effect). In addition, if the DMI is nonzero and the two nearest-neighbor coupling of J_1 and J_2 are different, as shown in Fig. 4(a), the Chern numbers of top and bottom bands are topologically nontrivial, the magnon energies and band gaps at $\boldsymbol{K}$ and $\boldsymbol{K}'$ become unequal and the valley splitting offers an energy window for realizing valley-selective magnon excitation by a magnon waveguide.

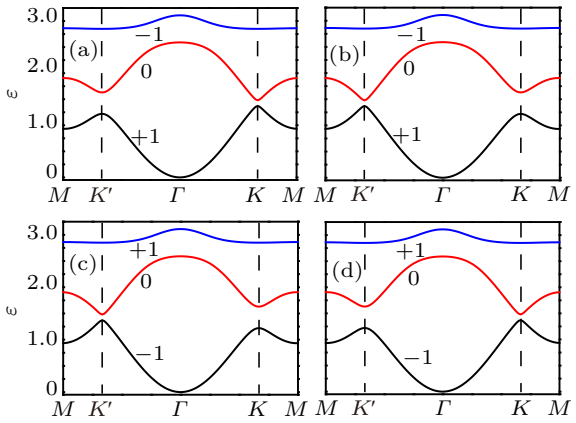


Fig. 4. The dispersion relations of periodic kagome strip lattices with DMI and nearest-neighbor couplings of J_1 and J_2. The parameters are (a) $D = 0.1$, $J_1 = 1.0$, $J_2 = 0.9$, (b) $D = 0.1$, $J_1 = 0.9$, $J_2 = 1.0$, (c) $D = 0.1$, $J_1 = 1.0$, $J_2 = 0.9$ and (d) $D = 0.1$, $J_1 = 0.9$, $J_2 = 1.0$. The Chern numbers of three bonds are indicated by 0, ± 1, respectively.

Indeed, experimental strategies for controlling the DMI direction can be applied in a synergistic manner to achieve precise control over this interaction, which is crucial for the development of advanced spintronic devices and magnetic memory technologies. Such as the interface engineering, chemical doping, strain engineering, electric field control, temperature control, magnetic field application or micromagnetic simulations. By combining these strategies, researchers can achieve a high level of control over the DMI, which is vital for the development of magnetic devices with tailored properties. Modification of the layer thickness, introducing interfacial roughness or adding buffer layers can also change the sign of the DMI. When exchanging J_1 and J_2 ($J_1 \leftrightarrow J_2$) or reversing the DMI (i.e., $D \to -D$), which is equivalent to the time reversal transformation in this case, it is observed that the magnitudes of the band gaps are interchanged between two valleys. Comparison of Fig. 4(a), when only J_1 and J_2 are exchanged, which is equivalent to a spatial inversion operation, with Fig. 4(b) shows that although the position of the energy valley has changed the Chern numbers of top and bottom bands are unchanged.

If only the DMI is reversed, as shown in Fig. 4(c), the position of the energy valley and the Chern number of the energy bands are both changed. When exchange of J_1 and J_2 and reversal of DMI are executed, as shown in Fig. 4(d), the magnitudes of the band gaps are unchanged at the two valleys. The above operation is a combination of spatial and time reversal symmetries. Naturally, the Chern numbers will exhibit a sign change. From this, it is clear that the valley physics is fully determined by the sign of the DMI strength and the relative magnitude of the SEI. For a positive $D(J_1 - J_2)$, the large and small gaps are localized at the $\boldsymbol{K}$ and $\boldsymbol{K}'$ valleys, respectively. The Dirac point of the edge modes is closer to the valley with the smaller gap. For a negative sign, the relative gap sizes are interchanged. Therefore, the location of the Dirac point is determined by the sign of $D(J_1 - J_2)$.

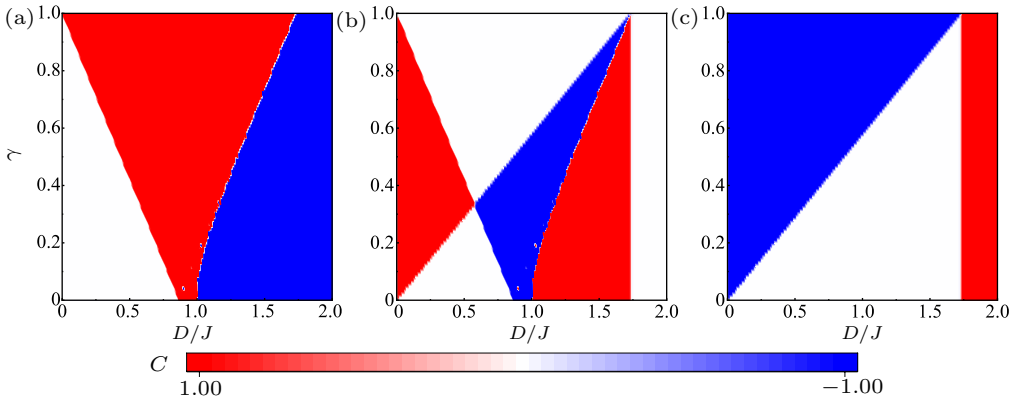


Fig. 5. The phase diagram of the Chern numbers of the three magnon bands versus D and γ. Red, white and blue correspond to Chern numbers of 1, 0 and -1, respectively, and (a), (b) and (c) correspond to the bottom, middle and top bands, respectively. There are some errors near the topological phase transitions due to the divergence of Berry curvature at the critical points.

For a kagome AB lattice, with changing DMI and γ, a few topological phase transitions can be observed. The topological phase diagrams of Chern numbers as functions of D and γ are shown in Fig. 5, which shows a few lines of critical points where two bands will touch and split and topological phase transitions appear. For the strengths of D and γ, the Chern numbers of three magnon bands have a discrete value of ± 1 or 0 and a boundary between the regions with different Chern numbers corresponds to a vanishing band gap. When moving through the boundary, there is a topological phase transition with an exchange of the band ordering, as shown in Fig. 3. In this process, decrease, closure and reopening of the band gap occur in turn. For the lower two bands, band exchange appears at the $\boldsymbol{K}$ and $\boldsymbol{K}'$ valleys. In contrast, it appears at the Γ point for the upper bands. For the isolated lowest band it is easy to find phase transitions from two limits. As D and γ increase, band switching occurs at $\boldsymbol{K}$, resulting in varied Chern numbers, while in the absence of band switching the gap at $\boldsymbol{K}'$ always increases. Therefore, the Chern number is determined by the relative magnitudes of D and γ.

4. Conclusion and perspectives

In conclusion, we have studied valley magnons and their topological properties in a kagome lattice. Valley degeneracy and band topology are tunable by DMI and SEI. We show that with nonzero DMI in a kagome AB lattice the magnon Hall effect can be observed from only one valley. Furthermore, we have demonstrated that reversing the DMI and exchange of J_1 and J_2 can also regulate the position of the unequal valleys; more strikingly, the jump of the Chern number of the magnon band to $+1$ and -1 only occurs when the direction of DMI changes. With increasing D and γ, a series of topological phase transitions appear when two bands come to touch and split at valleys. The magnon valley Hall effect and topological phase transitions provide new opportunities for designing energy-efficient spintronic and valleytronic devices.

Acknowledgements

We thank Lifa Zhang and Haiyang Zhang for helpful discussions. We acknowledge support from the Funding for School-level Research Projects of Yancheng Institute of Technology (Grant Nos. xjr2020038, xjr2022039, and xjr2022040).

References

[1] Dzyaloshinskii I 1958 *J. Phys. Chem. Solids* **4** 241
[2] Moriya T 1960 *Phys. Rev.* **120** 91
[3] Katsura H, Nagaosa N and Lee P A 2010 *Phys. Rev. Lett.* **104** 066403
[4] van Hoogdalem K A, Tserkovnyak Y and Loss D 2013 *Phys. Rev. B* **87** 024402
[5] Matsumoto R and Murakami S 2011 *Phys. Rev. Lett.* **106** 197202
[6] Cheng R, Okamoto S and Xiao D 2016 *Phys. Rev. Lett.* **117** 217202
[7] Zyuzin V Z and Kovalev A A 2016 *Phys. Rev. Lett.* **117** 217203
[8] Zhang L, Ren J, Wang J S and Li B W 2013 *Phys. Rev. B* **87** 144101
[9] Hasan M and Kane C 2010 *Rev. Mod. Phys.* **82** 3045
[10] Qi X and Zhang S 2011 *Rev. Mod. Phys.* **83** 1057
[11] Shindou R, Matsumoto R, Murakami S and Ohe J I 2013 *Phys. Rev. B* **87** 174427
[12] Mook A, Henk J and Mertig I 2014 *Phys. Rev. B* **90** 024412
[13] Mook A, Henk J and Mertig I 2016 *Spintronics IX. International Society for Optics and Photonics* **9931** 993134
[14] Mena M, Perry R, Perring T, Guerrero M Le S, Storni M, Adroja D, Ruegg C and McMorrow D 2014 *Phys. Rev. Lett.* **113** 047202
[15] Chisnell R, Helton J S, Freedman D E, Singh D K, BeWley R I, Nocera D G and Lee Y S 2015 *Phys. Rev. Lett.* **115** 147201
[16] Kruglyak V V, Demokritov S O and Grundler D 2010 *J. Phys. D* **43** 264001
[17] Owerre S A 2017 *J. Phys. Commun.* **1** 025007
[18] Li K, Li C, Hu J, Li Y and Fang C 2017 *Phys. Rev. Lett.* **119** 247202
[19] Su Y, Wang X S and Wang X R 2017 *Phys. Rev. B* **95** 224403
[20] Li F, Li Y, Kim Y, Balents L, Yu Y and Chen G 2016 *Nat. Comm.* **7** 12691
[21] Owerre S A 2016 *J. Phys.: Condens. Matter* **28** 386001
[22] Kim S K, Ochoa H, Zarzuela R and Tserkovnyak Y 2016 *Phys. Rev. Lett.* **117** 227201
[23] Katsura H, Nagaosa N and Lee P A 2010 *Phys. Rev. Lett.* **104** 066403
[24] Zeng K Y, Song F Y, *et al.* 2022 *Chin. Phys. Lett.* **39** 107501
[25] Sebastin A D, Jelena K and Loss D 2019 *Phys. Rev. Lett.* **122** 187203
[26] Kawano M and Hotta C 2019 *Phys. Rev. B* **99** 054422
[27] Xiao D, Yao W and Niu Q 2007 *Phys. Rev. Lett.* **99** 236809
[28] Yao W, Xiao D and Niu Q 2008 *Phys. Rev. B* **77** 235406
[29] Xiao D, *et al.* 2012 *Phys. Rev. Lett.* **108** 196802
[30] Xing Y H, Xu X F and Zhang L F 2017 *Acta Phys. Sin.* **66** 226601 (in Chinese)
[31] Mak K F, McGill K L, Park J and McEuen P L 2014 *Science* **344** 1489
[32] Lee J, Mak K F and Shan J 2016 *Nat. Nanotech.* **11** 421

[33] Gorbachev R, Song J, Yu G, Kretinin A, Withers F, Cao Y, Mishchenko A, Grigorieva I, Novoselov K, Levitov L S and Geim A 2014 *Science* **346** 448
[34] Owerre S A 2016 *J. Phys.: Condens. Matter* **28** 386001
[35] Kim S K, Ochoa H, Zarzuela R and Tserkovnyak Y 2016 *Phys. Rev. Lett.* **117** 227201
[36] Cao X, Chen K and He D 2015 *J. Phys.: Condens. Matter* **27** 166003
[37] Ideue T, Onose Y, Katsura H, Shiomi Y, Ishiwata S, Nagaosa N and Tokura Y 2012 *Phys. Rev. B* **85** 134411
[38] Onose Y, Ideue T, Katsura H, Shiomi Y, Nagaosa N and Tokura Y 2010 *Science* **329** 297
[39] Zhai X C and Blanter Y M 2020 *Phys. Rev. B* **102** 075407
[40] Hidalgo-Sacoto R, González R I, *et al.* 2020 *Phys. Rev. B* **101** 205425
[41] Heisenberg W 1928 *Z. Phys.* **49** 619
[42] Bose I and Bhaumik U 1994 *J. Phys.: Condens. Matter* **6** 10617
[43] Chernyshev A L and Maksimov P A 2016 *Phys. Rev. Lett.* **117** 187203
[44] Su Y, Wang X S and Wang X R 2017 *Phys. Rev. B* **95** 224403
[45] Rckriegel A, Brataas A and Duine R A 2018 *Phys. Rev. B* **97** 081106
[46] Xing Y H, Ma F S, Zhang L F and Zhang Z Y 2020 *Sci. China-Phys. Mech. Astron.* **63** 107511
[47] Xing Y H, Chen H, Xu N, Li X and Zhang L F 2022 *Phys. Rev. B* **105** 104409
[48] Li K K 2023 *Chin. Phys. Lett.* **40** 027502
[49] Shores M P, Nytko E A, Bartlett B M and Nocera D G 2005 *J. Am. Chem. Soc.* **127** 13462
[50] Olariu A, Mendels P, Bert F, Duc F, Trombe J C, deVries M A and Harrison A 2008 *Phys. Rev. Lett.* **100** 087202
[51] Colman R H, Ritter C and Wills A S 2008 *Chem. Mater.* **20** 6897
[52] Holstein T and Primakoff H 1940 *Phys. Rev.* **58** 1098
[53] Zhang L F, Wang J S and Li B W 2008 *Phys. Rev. B* **78** 144416
[54] Zhang L F and Niu Q 2015 *Phys. Rev. Lett.* **115** 115502